Treatment of Acute Kidney Injury Using a Dual Enzyme Embedded Metal-organic Framework-mediated Cascade That Catalyzes in Vivo ROS Scavenging

Xinyue Hou
Zhengzhou University
Jianxiang Shi
Zhengzhou University
Jie Zhang
Zhengzhou University First Affiliated Hospital
Zhigang Wang
Zhengzhou University First Affiliated Hospital
Sen Zhang
Zhengzhou University
Ruifeng Li
Zhengzhou University
Wei Jiang
Zhengzhou University
Jiancheng Guo
The Second Affiliated Hospital of Zhengzhou University
Wenjun Shang (fccshangwj@zzu.edu.cn)
Zhengzhou University First Affiliated Hospital

Research

Keywords: metal-organic frameworks, biomimetic mineralization, dual-enzyme cascade, ROS scavenging, acute kidney injury

Posted Date: May 18th, 2021

DOI: https://doi.org/10.21203/rs.3.rs-502119/v1

Abstract

Background: Significant advances have been made in recent years to utilize natural enzymes with antioxidant properties for the treatment of acute kidney injury (AKI). However, these enzymes have limited clinical utility due to their limited cellular uptake, poor pharmacokinetic properties, and suboptimal stability. We prepared a novel biomimetic mineralization approach to overcome these limitations.

Results: Catalase (CAT) and superoxide dismutase (SOD) were encapsulated in a zeolitic imidazolate framework-8 (ZIF-8), then this SOD@CAT@ZIF-8 complex was anchored with $MPEG_{2000}$-COOH to yield an $MPEG_{2000}$-SOD@CAT@ZIF-8 (PSCZ) composite. This composite was then utilized as a stable tool with antioxidant properties for the integrated cascade-based treatment of AKI, remarkably improved intracellular enzyme delivery. The PSCZ composite showed a significantly relieve ability of H_2O_2 induced ROS and prevented apoptosis in HEK293 cells. *In vivo*, this composite showed a protective effect in the cisplatin-induced AKI mouse model. In addition, PSCZ treatment mitigated renal dysfunction and histological injury, like tubulointerstitial infiltration. RNA sequencing results further confirmed the protective effect of PSCZ and the potential molecular mechanism was revealed. PSCZ treatment reduced renal inflammation and inflammatory gene expression and ameliorated increased apoptosis and inflammatory infiltration of renal tubules. Moreover, PSCZ administration regulated renal injury *via* the p53 signaling pathway. These renoprotective effects of PSCZ treatment were more potent in CP-AKI mice than those of SOD or CAT alone. This dual-enzyme-embedded metal-organic framework was able to scavenge reactive oxygen species synergistically and effectively.

Conclusion: PSCZ can remarkably improve intracellular enzyme delivery, and it can be used as a stable tool with antioxidant properties for the integrated cascade-based treatment of AKI. The ZIF-8-based “armor plating” represents an effective means of shielding enzymes with improved therapeutic utility to guide the precision medicine-based treatment of AKI.

Background

Acute kidney injury (AKI) is a severe condition wherein glomerular filtration is impaired, leading to the accumulation of nitrogenous waste in the systemic circulation. Over time, AKI can progress to end-stage renal disease (ESRD), which affects up to 20% of hospitalized patients and results in high morbidity and mortality rates. The pathogenesis of AKI is closely linked to reactive oxygen species (ROS) production, which can interact with nucleic acids and other macromolecules to induce inflammation and damage. While healthy kidney tissues can tolerate limited ROS levels without any adverse effects, excessive ROS production can trigger renal damage and eventually AKI. No effective clinical treatments for AKI have been developed to date, and majority patients have to seek supportive treatment via hemodialysis, peritoneal dialysis, and kidney transplantation. So how to prevent AKI plays a pivotal role in clinical settings.

A range of antioxidant enzymes, including superoxide dismutase (SOD), catalase (CAT), and reduced glutathione (GSH), function as ROS scavengers that can mitigate oxidative stress within a given cellular environment. Given that they are enzymes rather than small molecule therapeutics, these enzymes can catalyze the sustained conversion of toxic ROS species into less damaging byproducts, with SOD facilitating the conversion of $\bullet O_2$-into H_2O_2 and CAT then converting H_2O_2 into water and O_2. While they can function in concert with one another, CAT is primarily located within peroxisomes, whereas SOD is typically located in the cytosol or mitochondria, so additional transportation is necessary to facilitate H_2O_2 degradation. These endogenous enzyme systems show promise for in vivo therapeutic ROS scavenging and associated AKI treatment as effective and well-controlled antioxidants. Such enzymatic cascade reactions have advantages over conventional multi-stage reactions, reducing barriers to diffusion while increasing local intermediate concentrations to enhance overall reaction efficiency at a molecular level. These promising therapeutic properties have led many research groups to design enzymatic scaffold systems to mimic these efficient cascade systems in clinical settings. The *in vivo* application of these enzyme-based platforms would represent a key breakthrough with the potential to improve patient outcomes. However, several significant barriers currently limit the *in vivo* deployment of these enzyme-based systems, including the fact that they can readily undergo enzymatic degradation, are prone to enzyme aggregate formation, tend to lose catalytic activity throughout prolonged storage, and exhibit poor uptake by target cells owing to their negatively charged surfaces. Embedding or encapsulating these enzymes in a solid carrier framework thus offers an opportunity to overcome these delivery and stability limitations.

Metal-organic frameworks (MOFs) are novel biocompatible materials that exhibit tunable porosity and a high surface area, making them ideal for the packaging of candidate therapeutic biomolecules[1-3]. Traditionally, four primary strategies have been used for such packaging: grafting, infiltration, physical absorption, and encapsulation[4-7].

However, these approaches do not allow for precise control of the size of the generated biomacromolecular-MOF composites and are often highly inefficient. A recent biomimetic mineralization strategy has been developed to overcome these limitations[8], leveraging the fact that biomacromolecules exhibit an affinity for metal ions to conduct rapid macromolecule embedding a MOF through the stimulation of zeolitic imidazolate framework-8 (ZIF-8) growth. This approach can shield the enclosed macromolecules within a porous ZIF-8 exoskeleton capable of protecting against denaturation while permitting selective transportation through this porous network structure. ZIF-8 exoskeletal constructs are highly stable and biocompatible under physiological conditions, while they break down when exposed to the more acidic conditions found within solid tumors. Most studies of such MOF biocomposites to date have explored their use as biosensors or catalytic agents in aqueous or organic solutions[9-11]. The use of these MOFs to deliver proteins or nucleic acids is, in contrast, a relatively novel approach[12, 13]. To our knowledge, no prior studies described the biomimetic mineralization-based encapsulation of dual-enzyme within MOF crystals to enhance ROS scavenging. We hypothesized that a

ZIF-8 exoskeleton would be sufficient to protect SOD and CAT (SOD@CAT@ZIF-8), improve their stability, and thereby overcome the current barriers to alleviate ROS-mediated renal damage.

In the present study, we aim to develop a MOF encapsulating key antioxidant enzymes using a nanoscale ZIF-8 exoskeleton scaffold containing SOD and CAT (SOD@CAT@ZIF-8). This platform was further functionalized by anchoring $MPEG_{2000}$-COOH to the surface of the MOF complex, yielding more stable and biocompatible composites (**Scheme 1**). Relative to free CAT and SOD, this integrated $MPEG_{2000}$-SOD@CAT@ZIF-8 (PSCZ) platform exhibited greater SOD and CAT enzymatic efficiency *in vitro* and was found to synergistically enhance ROS scavenging *in vivo,* protecting mice against AKI-associated oxidative renal tissue damage. Together, our data indicate that MOF platforms incorporating integrated enzyme cascades offer great promise for the *in vivo* biomedical treatment of AKI and a range of other inflammatory conditions.

Materials And Methods

Materials

$Zn(NO_3)_2$•6(H_2O), 2-methyl imidazole (2-HmeIM), polyvinylpyrrolidone (PVP), SOD, CAT, and Fluorescein isothiocyanate (FITC) were purchased from Sigma-Aldrich and used as received. Methoxy-PEG-acid ($MPEG_{5000}$-COOH) and NH_2-PEG_{2000}-COOH were obtained from Ponsure Biological. Phosphate buffer solution (PBS) was obtained from Thermo-Fisher (Waltham, MA, USA). LysoTracker Green and Reactive Oxygen Species Assay Kit were purchased from Beyotime Company (China). All the aqueous solutions were prepared using purified deionized (DI) water purified with a purification system (Direct-Q3, Millipore, USA). The other solvents used in this work were purchased from Sinopharm Chemical Reagent (China) and Aladdin-Reagent (China).

Construction of SOD@CAT@ZIF-8 through biomimetic mineralization

Typically, 4 mL aqueous solution containing HMeIM (990 mg, 12 mM) was mixed with 4 mL of $Zn(NO_3)_2$•6(H_2O) solution (52 mg, 0.175 mM), 400 μL of SOD (10 mg) and CAT (10 mg) solution. The mixture was incubated at room temperature for 5 min, and then the solids were collected and washed with deionized water. The blue solids were subsequently dried at room temperature to obtain the composite SOD@CAT@ZIF-8. The SOD and CAT loading in ZIF-8 was calculated as follows:

Protein loading (%) = [(A - B) / A] × 100%

A and B represented the amount of protein in the initial solution and washing solution, measured based on the BCA assay.

Synthesis of PSCZ

$MPEG_{2000}$-COOH was connected to the surface of SOD@CAT@ZIF-8 through a coordination bond between -COOH group and the Zn ion to prepare PMs. Briefly, pre-formed CAT@SOD@ZIF-8 was dispersed in an $MPEG_{2000}$-COOH solution of 10 mg/mL using deionized water as the solvent. The mixture was sonicated for 10 min and stirred at room temperature for 48 h to form a PSCZ suspension. The white product was collected by centrifugation, followed by washing more than three times with deionized water and drying at 35 °C under vacuum.

Superoxide anion scavenging with PSCZ

The superoxide anion scavenging activity was assessed with a SOD assay kit (Solarbio, China). The $MPEG_{2000}$-SOD@CAT@ZIF-8 (PSCZ), $MEPG_{2000}$-SOD@ZIF-8 (PSZ), $MPEG_{2000}$-CAT@ZIF-8 (PCZ) concentrations (100 μg/mL) test was performed according to the instructions provided with the kit. The absorbance at 560 nm was measured using a quartz colorimetric dish reader after incubating at 37 °C for 30 min.

PSCZ scavenger hydrogen peroxide

The superoxide anion scavenging activity was assessed with a CAT assay kit (Solarbio, China). The PSCZ, PSZ, PCZ concentrations (100 μg/mL) test was performed according to the instructions provided with the kit. The absorbance at 405 nm was measured using a quartz colorimetric dish reader after incubating at room temperature for 10 min.

Viability of Cells Protected by PSCZ from Oxidative Stress

Human embryonic kidney 293 (HEK293) was cultured in Dulbecco's Modified Eagle Medium (DMEM) (1% penicillin/streptomycin and 10% fetal bovine serum) at 37°C under 5% CO_2. Using an RTCA E-Plate, HEK293 cells were seeded at a concentration of $1x10^4$ cells per well and incubated for 24 h. Next, PSCZ, PSZ, and PCZ dispersed in the cell culture medium at various concentrations (5,10,20 μg/mL) were added to the wells and incubated for 1 h. H_2O_2 was then added to the cells to a final concentration of 200μm and incubated for 24 h. Cells without any treatment and treated with only H_2O_2 were used as controls compared with only PSCZ, PSZ, and PCZ. The standard RTCA analysis is used to measure cell viability.

PSCZ scavenging of reactive oxygen species *in vitro*

2',7'-Dichlorofluorescin diacetate (DCFH-DA, D6883, Sigma-Aldrich, USA), an oxidation-sensitive fluorescent dye, was used to detect the intracellular ROS level according to the literature. Briefly, DCFH-DA is a non-fluorescent chemical compound that could freely diffuse through the cell membrane and be hydrolyzed by intracellular esterase to DCFH. The intracellular ROS could oxidize the non-fluorescent DCFH to fluorescent DCF. Therefore, the quantity of intracellular ROS is correlated with the fluorescent intensity of DCF. After incubation with H_2O_2 for 24 h, cells were gently rinsed thrice with a serum-free medium to remove the free PSCZ. Then, a final concentration of 10 μM of DCFH-DA in serum-free medium was added to the cells and incubated in the dark at 37 °C for 30 min. Afterward, the cells were

washed with serum-free medium thrice to remove the unloaded DCFH-DA probe, then were scanned using a laser confocal microscope (Zeiss LSM780, Germany). Flow cytometry analysis was used to quantify the intracellular ROS levels.

Furthermore, cells seeded in 6-well plates were stained with Annexin V-FITC apoptosis detection kit (A211-01, Vazyme, China) to detect the ratio of apoptotic and necrotic cells. Briefly, HEK293 cells in a well were collected, washed with cold PBS, and re-suspended in 195 μL binding buffer after incubation with H_2O_2 for 24 h. Then, 5 μL Annexin V-FITC and 10 μL PI were sequentially added to the cell suspension and incubated at room temperature in the dark for 15 min. After that, cells were analyzed by the Flow cytometer (NovoCyte, Agilent, USA). At least 50,000 cells were analyzed in each sample.

Finally, we used the mitochondrial membrane potential detection kit JC-1 (C2006, Beyoyime, China) probe method to detect mitochondrial membrane potential changes. HEK293 cells were seeded separately into confocal laser Petri dishes. Follow the instructions provided with the kit. After incubation with H_2O_2 for 24 h, cells were gently rinsed thrice with PBS to remove the free PSCZ. Then add 1 mL of JC-1 dye solution and mix well. Then the cells were incubated in an incubator at 37℃ for 20 min. An appropriate amount of JC-1 staining buffer (1×) was prepared by adding 1 mL of JC-1 staining buffer (5×) to 4 mL of distilled water and placed in an ice bath during incubation. At the end of incubation at 37℃, the supernatant was aspirated, washed twice with JC-1 staining buffer (1×), and then 2 mL cell culture solution was added, which could contain serum and phenol red. Finally, using a laser confocal microscope (Zeiss LSM780, Germany).

PSCZ scavenging of reactive oxygen species *in vitro*

Cisplatin-Induced AKI model

Female BALB/c mice aged 6-8 weeks were selected, all mice were received intraperitoneal injections of cisplatin (20 mg/kg). 24 h after injections, the mice in each group were sacrificed to monitor the model development. The blood samples and renal tissues were obtained and analyzed. The mice were intravenously injected with PSCZ (15 mg/kg in 100 μL PBS) at 1 h after intraperitoneal injections of cisplatin for the treatment group.

Treatment of CP-AKI Mice

One hour after the AKI model induction, different treatments were performed on AKI model mice: group 1 was healthy mice (n = 5); group 2 was AKI mice (PBS, n = 5); group 3 was AKI mice treated with 1× PBS (n = 5); group 4 was AKI mice treated with PSCZ (15 mg/kg in 100 μL PBS, n = 5). After 24 h p.i, blood samples and tissues of each organ were collected, the treatment group was compared with healthy mice to evaluate kidney function.

Kidney function test

After euthanizing the mice, blood samples were collected in lithium heparin tubes. The blood serum was collected after centrifuging the blood samples at 2000 g for 15 min at 4℃. Finally, the samples were sent to the Laboratory Department of the First Affiliated Hospital of Zhengzhou University for analysis of blood urea nitrogen (BUN) levels and blood creatinine (CRE) levels.

Haemotoxylin and Eosin (H&E) Staining of Kidney Sections

In the AKI model and time-point of interest, mice were euthanized, and the kidneys were collected and fixed with paraformaldehyde (4% in PBS). Laboratory Animal Center of Zhengzhou University embedded the samples in paraffin wax, sliced, and then stained with H&E stain.

Analysis of the therapeutic effect in renal tissue

Kidneys from each group were snap-frozen and stored at 80℃ until use. Kidney homogenates were prepared according to the protocols of different assays. SOD level and CAT level were assessed with a SOD assay kit and CAT assay kit (Sigma-Aldrich, USA). To evaluate ROS's scavenging effect histologically, each group's kidney tissues were removed and stored in a refrigerator at -80 ℃ until use. Kidney tissues of mice in each group were sliced using a frozen micro-slicer. Frozen kidney tissue slides (about 5μm thickness) were washed with PBS and stained with 1 mM DCFH-DA for 30 min to detect superoxide formation. Then a cover glass was applied to each slide using Vectashield mounting medium. Finally, a laser confocal microscope was used to observe the fluorescence changes. The other part of the tissue was frozen and sliced in the same way, then stained with TNFα- and IL1β antibodies and DAPI. After staining, the tissue was observed under the confocal microscope.

RNA sequencing

Mice were sacrificed to harvest the kidneys. The kidneys were washed thrice with saline and snap-frozen in liquid nitrogen. Total RNA was extracted by using the TIANGEN Animal Tissue Total RNA Extraction Kit (DP419, TIANGEN, China). RNA integrity was verified by Agilent 4200 Bioanalyzer and quantified using ND-2000 (Nanodrop Technology). Cell rRNA was removed by using MGIEasy rRNA removal kit. Library construction was carried out using the MGIEasy RNA Library Prep Set (96 RXN) according to the manufacturer's protocol. Libraries were visualized on the Agilent 4200 Bioanalyzer to check insert size and quantified by using the Qubit Fluorometers to determine the concentration. Libraries were pooled and loaded on the flow cell to run on MGISEQ-2000 sequencer as paired-end read for 150 cycles on each side.

Bioinformatics analysis

Transcriptomics sequencing and mapping

Clean reads were mapped to Mus musculus reference genome (GRCm38) with STAR aligner (version 2.6.1d).[34] Transcript-level gene expression was estimated by Salmon (version 0.14.1).[35] Transcript per million (TPM) values were calculated using tximport. A community-developed pipeline called bcbio-nextgen was used to automate the upstream bioinformatic analysis.[36]

Identification and functional annotation of differentially expressed genes (DEGs)

The R package bcbioRNASeq can take the bcbio-nextgen output as input and generate count matrices, identify DEGs, conduct functional annotations and visualize the results.[37] DEGs were identified for each group compared with the control group using DESeq2,[38] with a fold-change threshold of 1 and *P* values cutoff of 0.05. Functional annotation of DEGs was performed using the clusterProfiler R package to identify associated pathways in AKI.[39] We further explored the mechanism of AKI and whether PSCZ can reverse the unfavorable changes in transcriptional level.

Characterization

T Fourier transforms infrared spectra (FT-IR) were measured on a Shimadzu FTIR 8400S spectrometer. Scanning electron microscopy (SEM) images were captured on a Hitachi FE-SEM S-4800 instrument with an acceleration voltage of 3 kV. The samples were prepared by depositing sample dispersion onto a freshly cleaved silicon wafers surface. Powder X-ray diffraction (PXRD) patterns were collected on a PANalytical B.V. Empyrean powder diffractometer, in which data were collected from 5^{o} to 45^{o} at a scan rate of 15 ^{o}/min.

Results And Discussion

Synthesis and characterization of PSCZ

As shown in Scheme 1, the native enzyme could be embedded in a porous nanomaterial ZIF-8, in which $Zn(OAc)_2$, 2-HMeIM, SOD, and CAT were incubated for 5 min at room temperature. The morphology of composite SOD@CAT@ZIF-8 and PSCZ was characterized by SEM (**Figure 1A**). The SEM image showed that SOD@CAT@ZIF-8 and PSCZ both possessed uniform rhombic dodecahedral morphology similar to blank ZIF-8. As shown in **Figure 1B,** the PXRD pattern of PSZ, PCZ, and PSCZ both exhibited peaks matching well with the simulated ZIF-8 suggesting that ZIF-8 frameworks were formed in the biomimetic mineralization, and the structural integrity of ZIF-8 could be retained in the presence of SOD and CAT. FT-IR spectra of PSZ, PCZ, and PSCZ characteristic with $MPEG_{2000}$-COOH peaks at 2865–2875 cm^{-1} that were respectively attributable to -COOH and $-OCH_3$, indicating the successful conjunction of $MPEG_{2000}$. We further investigated the antioxidant activities of PSCZ, PSZ, and PCZ. Among biologically relevant ROS, H_2O_2 is of greatest importance because of its membrane permeability, longer half-life than O^{2-} and ·OH, and consequently highest intracellular concentration. As shown in **Figure 1E and 1F**, we investigated the cascading enzyme scavenging ability of PSCZ, a remarkable difference in the activity was observed. PSCZ showed enhanced antioxidant activities in both SOD- and CAT-like activities.

Assessment of the ability of PSCZ to scavenge ROS *in vitro*

Given the promising properties of PSCZ particles as stable, biocompatible antioxidant agents, we next assessed their ROS scavenging activity *in vitro* relative to that of free CAT and SOD. Given that AKI pathogenesis is associated with oxidative damage to the renal tubules, we utilized the HEK293 cell line

model to assess the ability of PSCZ to protect against ROS-mediated injury [14]. We additionally utilized an xCELLigence (RTCA) instrument to monitor the survival and growth of these cells in a quantitative, real-time, dynamic manner. This assay approach is superior to traditional endpoint-based viability assays that assess membrane permeability [15], enabling the assessment of cell survival in a label-free and automated manner throughout a given experimental period [16]. RTCA approach was used to measure the survival and growth of cells over a 24 h period following treatment with H_2O_2 and these different nanoenzymes preparations. PSCZ showed superior antioxidant capacity at 5 µg/mL than PSZ and PCZ even at a higher (20 µg/mL) concentration (**Figure 2A**). We then treated HEK293 cells with H_2O_2 to induce oxidative stress to evaluate the ability of PSCZ to protect against oxidative damage (**Figure 2B**). While the viability of H_2O_2-treated cells was ~50%, PSCZ treatment was associated with a significant increase in these cells' survival due to the observed reductions in intracellular ROS production and the consequent preservation of mitochondrial functionality (**Figure 2B**).

We also utilized the DCFH-DA fluorescent probe to assess intracellular ROS levels to further confirm whether PSCZ could suppress H_2O_2-induced ROS generation in HEK293 cells. While a significant increase in DCFH-DA fluorescence was evident in H_2O_2-treated cells relative to untreated controls (**Figure 2D**), this fluorescence intensity was significantly reduced in cells that had additionally been treated with PSCZ. This finding was further confirmed via flow cytometry **(Figure 2C)**, revealing that PSCZ could reliably suppress H_2O_2-mediated free radical generation.

Mitochondrial oxidative phosphorylation is the primary mechanism whereby most cells produce ATP [17]. Given that renal PTECs lack glycolytic activity and are under high metabolic energy demands, these cells exist under conditions of ischemia and hypoxia [18]. This increases the susceptibility of these renal tubular epithelial cells to acute renal injury. Mitochondria are also central regulators of intracellular apoptotic signaling, with the loss of mitochondrial membrane potential (Δψm) being an early apoptotic indicator [19]. Therefore, we assessed the impact of PSCZ on HEK293 cell Δψm using a JC-1 staining approach, with a higher red/green JC-1 ratio indicative of lower levels of mitochondrial dysfunction. We observed a significant decrease in the Δψm of these cells following H_2O_2 treatment (**Figure S1**), whereas PSCZ treatment yielded a JC-1 fluorescence ratio comparable to that in control cells, suggesting that PSCZ can preserve mitochondrial membrane integrity.

Excess ROS generation can initiate apoptotic signaling cascades within cells [20, 21]. Given the acute sensitivity of renal tubule cells to oxidative damage, we next assessed the ability of PSCZ to facilitate *in vitro* ROS scavenging activity in our HEK293 cell model system. When the death of these cells was assessed *via* flow cytometry following Annexin V/PI staining, we found that H_2O_2 treatment (200 µm) increased the frequency of apoptotic HEK293 cells to 36.43%, relative to control cells (3.28%) (**Figure 3**). In contrast, cells treated with H_2O_2 and PSCZ exhibited significantly lower rates of apoptotic death (6.43%). These findings thus confirmed that PSCZ could protect against oxidative damage in HEK293 cells *in vitro.*

PSCZ effectively facilitates *in vivo* ROS scavenging

Given the promising *in vitro* results detailed above, we next explored the *in vivo* utility of our MOF antioxidant platform using a murine cisplatin-induced AKI (CP-AKI) model system [22]. Cisplatin (CDDP) is a widely used chemotherapeutic drug that accumulates within renal proximal tubule epithelial cells (PTECs), resulting in localized renal inflammation, damage, apoptotic death, and AKI that can manifest in the form of CDDP-associated nephrotoxicity [23]. The pathogenesis of CP-AKI has been linked to ROS production and consequent acute tubular apoptosis [24]. Thus, this CP-AKI model system was selected for further analyses of the relative safety and *in vivo* antioxidant activity of PSCZ.

CP-AKI mice were established as in prior reports by intraperitoneally injecting these animals with CDDP (20 mg/kg) and then measuring serum BUN and CRE levels after 24 h to gauge renal function [25], given that these compounds accumulate in the blood in the context of renal damage. Mice in corresponding treatment groups were intravenously treated with PSCZ 1 h before CDDP administration (**Figure 4A**). CRE and BUN levels were significantly higher in CP-AKI mice than healthy controls (**Figure 4B-C**), consistent with the successful induction of CDDP-mediated kidney damage in these animals. Saline infusions are commonly administered to patients before and during CDDP treatment [25], as such infusions exhibit poorly understood renoprotective activity against CDDP-induced nephrotoxicity. However, CP-AKI will manifest in roughly 30% of treated patients [26]. Our mouse model system observed comparable findings, as only slight reductions in CRE and BUN levels were observed in CP-AKI mice treated with PBS, with these levels being significantly higher than those in control animals. In contrast, the treatment of CP-AKI mice with PSCZ resulted in significant reductions in CRE and BUN levels to concentrations comparable to those in healthy control mice. These data underscored the therapeutic utility of PSCZ as a safe and effective tool for treating CP-AKI in mice.

We additionally isolated renal tissue sections from these treated mice and stained them with H&E stain to assess treatment-related changes in tissue pathology. Renal casts can arise due to denatured protein precipitation in kidney tubules and are often considered to be an indicator of kidney disease. Similarly, inflammatory cell infiltration and the formation of vacuoles within renal tubules can be visualized to detect and gauge the severity of the renal inflammatory injury. While many casts were evident in the renal tissue samples from CP-AKI model mice (**Figure 4D**), relatively few were detectable in AKI model animals that had been administered PSCZ, consistent with the ability of these nanoparticles to preserve the integrity of renal tissues better.

To further assess the ability of PSCZ to suppress renal ROS generation, we next used the fluorescent ROS probe DCFH-DA to stain kidney tissue sections from CP-AKI mice in our different treatment groups and then imaged these tissues via laser scanning confocal microscopy. This approach revealed that PSCZ administration significantly inhibited renal ROS accumulation in our AKI model mice (**Figure S2**).

Tumor necrosis factor-alpha (TNF-α) and interleukin-1β (IL-1β) are key inflammatory cytokines and drivers of apoptotic cell death in the context of cisplatin-induced renal injury [27, 28]. Excess ROS production by cells under inflammatory conditions can induce additional proinflammatory cytokine

production, thereby promoting further immune cell infiltration and renal damage. IL-1β can further amplify these inflammatory processes through feedback mechanisms [24]. Renal tissue samples from treated mice were collected and analyzed to reveal the underlying mechanism of PSCZ. Immunofluorescence results showed that IL-1β and TNF-α levels were comparable in the PSCZ-treated and control groups, suggesting these nanoparticles did not induce direct inflammation in mice at the utilized concentrations and can reduce inflammation-induced kidney damage (**Figure 5A-5D**). Notably, in AKI model mice, PSCZ administration suppressed TNF-α and IL-1β expression relative to untreated model controls. We additionally assessed SOD and CAT levels in renal homogenates from these mice **(Figure 5E and 5F)**, to confirm that these antioxidant enzymes were successfully delivered to damaged kidney tissue [29]. Excessive ROS levels can result in SOD and CAT depletion, as was evident in CP-AKI and PBS-treated mice. In contrast, PSCZ resulted in renal SOD and CAT levels similar to those in healthy control animals. It was confirmed that PSCZ was successfully delivered to the injured renal tissue and alleviated renal inflammatory injury.

To further test the therapeutic utility of PSCZ, we next measured malondialdehyde (MDA) levels and blood biochemical parameters to evaluate renal excretory function. MDA analysis results revealed that both CP-AKI mice and PBS-treated AKI mice exhibited elevated MDA levels consistent with renal failure, while PSCZ administration lowered these levels consistent with the alleviation of AKI-related renal damage **(Figure 5G)**. Analyses of blood biochemical parameters from these mice indicated that PSCZ treatment was not associated with obvious renal toxicity **(Figure 5H-5L)**, and hematological parameters in PSCZ-treated animals were comparable to those in healthy controls. These findings suggested that our PSCZ particles were highly biocompatible and useful as a tool for AKI treatment. However, it is essential to note that we only tested for acute toxicity associated with this therapeutic platform, and further research will be necessary to establish whether PSCZ is retained in the kidney beyond the 24 h time point, whether it is eliminated via renal metabolic processing, and whether it induces any long-term toxicity *in vivo.*

RNAs-seq analysis confirmed the successful construction of the AKI model and PSCZ showed a superior protective effect in the AKI mouse model

In the current study, we set four different groups: control group without any treatment (brief as the control group), cisplatin-induced AKI group (brief as CP-AKI group), AKI group pretreated with PSCZ (brief as the PSCZ+AKIgroup), and AKI group pretreated with PBS (brief as the PBS+CP-AKI group). More detailed information is shown in the M&M section.

An average of 63.34 (range from 58.51 to 66.33) million raw reads were obtained for all samples. After removing low-quality reads, an average of 60.52 (range from 56.05 to 63.16) million clean reads were retained for further analysis. The raw data were uploaded to National Omics Data Encyclopedia (NODE) database (https://www.biosino.org/node) with the following accession number OEP000285.

To further elucidate the underlining therapeutic mechanisms, CP-AKI was chosen as the representative disease model for further transcriptomic analysis. DESeq2 identified a total of 601, 157, and 88 DEGs for

the CP-AKI group, CP-AKI+PSCZ group, and CP-AKI+PBS group compared with the control group, respectively **(Figure 6D**). An unguided principal component analysis (PCA) of the data revealed different transcriptomic profiles between PSCZ and PBS-treated AKI mice kidneys (**Figure 6C**). The Venn diagram in **Figure 6B** showed many differentially expressed genes were produced in the CP-AKI group compared with the control group, and the differentially expressed genes were decreased in the PSCZ treatment group.

We also investigated the impact of PSCZ on gene expression related to growth arrest and DNA damage response, apoptosis, oxidation-reduction, etc. (**Figure 6G)**. In brief, the PSCZ treatment could reverse the impact of cisplatin-induced AKI in the mouse model.

DEGs in the CP-AKI group were enriched in the p53 signaling pathway, FoxO signaling pathway, apoptosis-related pathways, etc (**Figure 6E and F, Figure S3**). This is consistent with previous research. Cisplatin can interfere with DNA replication and DNA repair mechanisms, cause DNA damage, and induce apoptosis in cells.[30] Cisplatin can also increase cellular ROS and induce endoplasmic reticulum (ER) stress, contributing to cisplatin toxicity. Cell death and ER stress are characteristic of cisplatin-induced AKI.[26, 31] P53 signaling is an early-stage response to cisplatin toxicity in renal cells. Cisplatin caused renal cells to initiated the p53 dependent DNA repair pathway. .If ROS continues to be overproduced in renal cells, the intrinsic apoptotic pathway will be activated. In the early stage, when cisplatin interferes with DNA replication and DNA repair mechanism, nano inhibits the excessive production of ROS caused by cisplatin, promotes the initiation of DNA repair pathway, and alleviates renal cell damage(**Figure 6A, Figure S4**).

In the current study, the kidney proximal nephron tubule segment injury marker Havcr1 (also known as Kim1) slightly changed (log_2FC = 0.42, *adj. P* = 0.437) CP-AKI group compared with the control group. This is probably because the kidneys were harvested in the very early stage of AKI. This is consistent with a previous study that cisplatin-induced AKI mainly caused proximal nephron tubule segment injury in the very early stage.[32] *Bax*, *Bak1* are important signals in the apoptosis cascade and normally act on the mitochondrial membrane to promote permeabilization and release of cytochrome C and ROS. In CP-AKI group, *Bax* and *Bak1* significantly increased (log_2FC = 1.16, adj. *P* = 0.024; log_2FC = 0.99, adj. *P* = 0.048, respectively). This means that ROS level increased by cisplatin. *Aco1* and *Cyp2e1*, which are important oxidation-reduction enzymes, significantly decreased (log_2FC = -0.74, adj. *P* = 0.007; log_2FC = -1.03, adj. *P* = 0.026, respectively). This indicated that the normal function of oxidation-reduction was compromised. *Gadd45a* and *Gadd45b*, which are growth arrest and DNA damage response genes, also increased (log_2FC = 1.13, adj. *P* = 0.045; log_2FC = 1.29, adj. *P* = 0.024, respectively). This indicated that kidney cells responded to cisplatin-induced DNA damage by cell cycle arrest and initiated the DNA repair system, in which case, the p53 signaling pathway. *Tnfrsf12a* and *Tnfrsf10b* (also known as *Dr5*), which belong to tumor necrosis factor receptor superfamily and transduces apoptosis signals, significantly increased in CP-AKI group (log_2FC = 1.50, adj. *P* =0.003; log_2FC = 1.45, adj. *P* =0.006, respectively). *Caspase8* also significantly increased in CP-AKI group (log_2FC = 0.74, adj. *P* =0.044). This indicated that cisplatin-

induced intrinsic apoptosis through *Caspase8* by upregulating *Tnfrsf10b* in the CP-AKI group. The results indicated that the apoptosis process was initiated in the CP-AKI group even after 24 h being treated with cisplatin. *Bcl10* contains a caspase recruitment domain (*CARD*) and has been shown to induce apoptosis and activate NF-κB. *Bcl10* slightly increased in CP-AKI group ($log_2FC = 0.70$, adj. $P = 0.159$).

However, this process is reversible if cell oxidative stress can be alleviated. In PBS and PSCZ pretreated group, *Bax* and *Bak1* tended to return to normal level (*Bax*: $log_2FC = 0.89$, adj. $P = 0.260$; $log_2FC = 0.52$, adj. $P = 0.774$, respectively; Bak1: $log_2FC = 0.39$, adj. $P = 0.836$; $log_2FC = 0.11$, adj. $P = 1.000$, respectively), *Tnfrsf12a* and *Tnfrsf10b* also tended to return to normal level (*Tnfrsf12a:* $log_2FC = 0.54$, adj. $P = 0.500$; $log_2FC = 0.13$, adj. $P = 1.000$, respectively; *Tnfrsf10b:* $log_2FC = 0.99$, adj. $P = 0.177$; $log_2FC = 0.42$, adj. $P = 0.860$) compared with CP-AKI group. This indicated that renal cell oxidative stress was significantly ameliorated, and cell apoptosis was repressed. *Gadd45a* and *Gadd45b* also tended to return to normal level in PBS and PSCZ pretreated AKI mouse models (*Gadd45a*: $log_2FC = 0.35$, adj. $P = 0.897$; $log_2FC = -0.04$, adj. $P = 1.000$, respectively; *Gadd45b*: $log_2FC = 0.38$, adj. $P = 0.862$; $log_2FC = 0.33$, adj. $P = 0.957$, respectively). This indicated cell cycle arrest was also alleviated in both groups. Tadagavadi *et al.* also reported that PBS have protective effects in AKI models[33]. This is consistent with the findings in current study. Moreover, in current study, PSCZ showed superior protective effect than PBS.

Declarations

Ethics approval

The Ethics Committee of Experimental Animal Center of Zhengzhou University approved the animal experiment in this study, and the Ethics Approval Certificate number is ZZU-LAC20200703.

Consent for publication

All authors have reviewed the manuscript and approved the submission of this manuscript.

Availability of data and materials

All data associated with this study are present in the paper or the Supplementary Materials. RNA sequencing data can be accessed in the NODE database with the following URL (http://www.biosino.org/node/project/detail/OEP000285).

Competing interests

The authors declare that there is no conflict of interest.

Funding and Acknowledgements

We greatly appreciate the financial support from the National Natural Science Foundation of China (No. 81901882), China postdoctoral science foundation (2019M663062), Henan Province Medical Science

and Technology Public Relations Plan Province Department joint construction project (SBGJ2018041, LHGJ20190329), and Education Department of Henan Province (20A430026), the Collaborative Innovation Project of Zhengzhou (Zhengzhou University) (No. 20XTZX05014). Data analysis was supported by the Supercomputing Center in Zhengzhou University (Zhengzhou).

Authors' contributions

WJS, JCG, and **WJ** conceived the idea, provided funding support, interpreted the results, and critically revised and finalized the manuscript. **XYH:** designed and performed experiments, organized the data and wrote the manuscript. **JXS:** analyzed transcriptome sequencing data and interpreted results, wrote and revised the manuscript. **JZ:** constructed the mouse model and performed the experiments. **ZGW:** provided materials and helped to construct the mouse model. **SZ:** conducted molecular biological experiments. **RFL:** performed data analysis, generated figures, and organized data.

References

1. Lu K, Aung T, Guo N, Weichselbaum R, Lin W. Nanoscale Metal-Organic Frameworks for Therapeutic, Imaging, and Sensing Applications. Adv Mater. 2018;30:e1707634.
2. Simon-Yarza T, Giménez-Marqués M, Mrimi R, Mielcarek A, Gref R, Horcajada P, Serre C, Couvreur P. A Smart Metal-Organic Framework Nanomaterial for Lung Targeting. Angew Chem Int Ed Engl. 2017;56:15565–9.
3. Suresh K, Matzger AJ. Enhanced Drug Delivery by Dissolution of Amorphous Drug Encapsulated in a Water Unstable Metal-Organic Framework (MOF). Angew Chem Int Ed Engl. 2019;58:16790–4.
4. Feng D, Liu TF, Su J, Bosch M, Wei Z, Wan W, Yuan D, Chen YP, Wang X, Wang K, et al. Stable metal-organic frameworks containing single-molecule traps for enzyme encapsulation. Nat Commun. 2015;6:5979.
5. Shieh FK, Wang SC, Yen CI, Wu CC, Dutta S, Chou LY, Morabito JV, Hu P, Hsu MH, Wu KC, Tsung CK. Imparting functionality to biocatalysts via embedding enzymes into nanoporous materials by a de novo approach: size-selective sheltering of catalase in metal-organic framework microcrystals. J Am Chem Soc. 2015;137:4276–9.
6. Chen D, Suo M, Guo J, Tang W, Jiang W, Liu Y, Duo Y. Development of MOF "Armor-Plated" Phycocyanin and Synergistic Inhibition of Cellular Respiration for Hypoxic Photodynamic Therapy in Patient-Derived Xenograft Models. Adv Healthc Mater. 2021;10:e2001577.
7. Jiang W, Wang X, Chen J, Liu Y, Han H, Ding Y, Li Q, Tang J. Deuterohemin-Peptide Enzyme Mimic-Embedded Metal-Organic Frameworks through Biomimetic Mineralization with Efficient ATRP Catalytic Activity. ACS Appl Mater Interfaces. 2017;9:26948–57.
8. Liang K, Ricco R, Doherty CM, Styles MJ, Bell S, Kirby N, Mudie S, Haylock D, Hill AJ, Doonan CJ, Falcaro P. Biomimetic mineralization of metal-organic frameworks as protective coatings for biomacromolecules. Nat Commun. 2015;6:7240.

9. Sun CY, Qin C, Wang XL, Yang GS, Shao KZ, Lan YQ, Su ZM, Huang P, Wang CG, Wang EB. Zeolitic Imidazolate framework-8 as efficient pH-sensitive drug delivery vehicle. Dalton Trans. 2012;41:6906–9.
10. Wang Q, Zhang X, Huang L, Zhang Z, Dong S. GOx@ZIF-8(NiPd) Nanoflower: An Artificial Enzyme System for Tandem Catalysis. Angew Chem Int Ed Engl. 2017;56:16082–5.
11. Huang S, Kou X, Shen J, Chen G, Ouyang G. “Armor-Plating” Enzymes with Metal-Organic Frameworks (MOFs). Angew Chem Int Ed Engl. 2020;59:8786–98.
12. Zhuang J, Gong H, Zhou J, Zhang Q, Gao W, Fang RH, Zhang L. Targeted gene silencing in vivo by platelet membrane-coated metal-organic framework nanoparticles. Sci Adv. 2020;6:eaaz6108.
13. Zhuang J, Duan Y, Zhang Q, Gao W, Li S, Fang RH, Zhang L. Multimodal Enzyme Delivery and Therapy Enabled by Cell Membrane-Coated Metal-Organic Framework Nanoparticles. Nano Lett. 2020;20:4051–8.
14. Pavlakou P, Liakopoulos V, Eleftheriadis T, Mitsis M, Dounousi E. Oxidative Stress and Acute Kidney Injury in Critical Illness: Pathophysiologic Mechanisms-Biomarkers-Interventions, and Future Perspectives. Oxid Med Cell Longev. 2017;2017:6193694.
15. Yah CS, Simate GS. Engineered nanoparticle bio-conjugates toxicity screening: The xCELLigence cells viability impact. Bioimpacts. 2020;10:195–203.
16. Çetin İ, Topçul MR. Evaluation of the cytotoxic effect of Ly2109761 on HeLa cells using the xCELLigence RTCA system. Oncol Lett. 2019;17:683–7.
17. Xu Y, Fei J, Li G, Yuan T, Xu X, Li J. Nanozyme-Catalyzed Cascade Reactions for Mitochondria-Mimicking Oxidative Phosphorylation. Angew Chem Int Ed Engl. 2019;58:5572–6.
18. Yu B, Wei H, He Q, Ferreira CA, Kutyreff CJ, Ni D, Rosenkrans ZT, Cheng L, Yu F, Engle JW, et al. Efficient Uptake of (177) Lu-Porphyrin-PEG Nanocomplexes by Tumor Mitochondria for Multimodal-Imaging-Guided Combination Therapy. Angew Chem Int Ed Engl. 2018;57:218–22.
19. Sastre J, Pallardó FV, García de la Asunción J, Viña J. Mitochondria, oxidative stress and aging. Free Radic Res. 2000;32:189–98.
20. Meng XM, Ren GL, Gao L, Yang Q, Li HD, Wu WF, Huang C, Zhang L, Lv XW, Li J. NADPH oxidase 4 promotes cisplatin-induced acute kidney injury via ROS-mediated programmed cell death and inflammation. Lab Invest. 2018;98:63–78.
21. Ratliff BB, Abdulmahdi W, Pawar R, Wolin MS. Oxidant Mechanisms in Renal Injury and Disease. Antioxid Redox Signal. 2016;25:119–46.
22. Rewa O, Bagshaw SM. Acute kidney injury-epidemiology, outcomes and economics. Nat Rev Nephrol. 2014;10:193–207.
23. Manohar S, Leung N. Cisplatin nephrotoxicity: a review of the literature. Journal of Nephrology. 2018;31:15–25.
24. Ozkok A, Edelstein CL. Pathophysiology of Cisplatin-Induced Acute Kidney Injury. Biomed Res Int. 2014;2014:967826.

25. Sharp CN, Siskind LJ. Developing better mouse models to study cisplatin-induced kidney injury. Am J Physiol Renal Physiol. 2017;313:F835-f841.
26. Sharp CN, Doll MA, Dupre TV, Shah PP, Subathra M, Siow D, Arteel GE, Megyesi J, Beverly LJ, Siskind LJ. Repeated administration of low-dose cisplatin in mice induces fibrosis. American Journal of Physiology-Renal Physiology. 2016;310:F560–8.
27. Schieber M, Chandel NS. ROS function in redox signaling and oxidative stress. Curr Biol. 2014;24:R453–62.
28. Martindale JL, Holbrook NJ. Cellular response to oxidative stress: signaling for suicide and survival. J Cell Physiol. 2002;192:1–15.
29. Hao C, Qu A, Xu L, Sun M, Zhang H, Xu C, Kuang H. Chiral Molecule-mediated Porous Cu (x)O Nanoparticle Clusters with Antioxidation Activity for Ameliorating Parkinson's Disease. J Am Chem Soc. 2019;141:1091–9.
30. Dasari S, Tchounwou PB. Cisplatin in cancer therapy: molecular mechanisms of action. Eur J Pharmacol. 2014;740:364–78.
31. Sharp CN, Siskind LJ. Developing better mouse models to study cisplatin-induced kidney injury. American Journal of Physiology-Renal Physiology. 2017;313:F835–41.
32. Bolisetty S, Traylor A, Joseph R, Zarjou A, Agarwal A. Proximal tubule-targeted heme oxygenase-1 in cisplatin-induced acute kidney injury. American Journal of Physiology-Renal Physiology. 2016;310:F385–94.
33. Tadagavadi RK, Reeves WB. Renal dendritic cells ameliorate nephrotoxic acute kidney injury. J Am Soc Nephrol. 2010;21:53–63.
34. Dobin A, Davis CA, Schlesinger F, Drenkow J, Zaleski C, Jha S, Batut P, Chaisson M, Gingeras TR. STAR: ultrafast universal RNA-seq aligner. Bioinformatics. 2013;29:15–21.
35. Patro R, Duggal G, Love MI, Irizarry RA, Kingsford C. Salmon provides fast and bias-aware quantification of transcript expression. Nature methods. 2017;14:417–9.
36. Guimera RV. bcbio-nextgen: Automated, distributed next-gen sequencing pipeline. EMBnet journal. 2011;17:30.
37. Steinbaugh MJ, Pantano L, Kirchner RD, Barrera V, Chapman BA, Piper ME, Mistry M, Khetani RS, Rutherford KD, Hofmann O: **bcbioRNASeq**: **R package for bcbio RNA-seq analysis**. *F1000Research* 2018, **6**:1976.
38. Love MI, Huber W, Anders S. Moderated estimation of fold change and dispersion for RNA-seq data with DESeq2. Genome biology. 2014;15:1–21.
39. Yu G, Wang L-G, Han Y, He Q-Y. clusterProfiler: an R package for comparing biological themes among gene clusters. Omics: a journal of integrative biology. 2012;16:284–7.

Figures

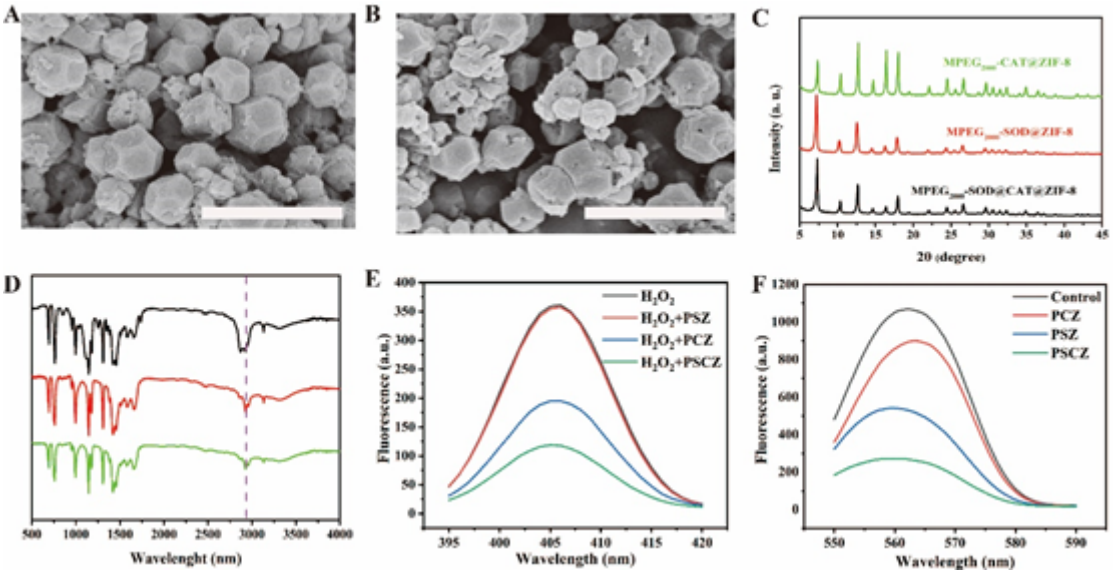

Figure 1

A) SEM images of SOD@CAT@ZIF-8 and PSCZ following rinsing using dH2O; scale bar = 1 μm; C) Powder X-ray diffraction (PXRD) patterns of PSZ, PCZ, and PSCZ; D) Fourier transform infrared spectra (FT-IR) of PSZ (green), PCZ (red), and PSCZ (black); E) Percent inhibition decomposition of H2O2 with PSZ, PCZ, and PSCZ; F) SOD-like activity of PSZ, PCZ, and PSCZ with concentration (100 μg/mL).

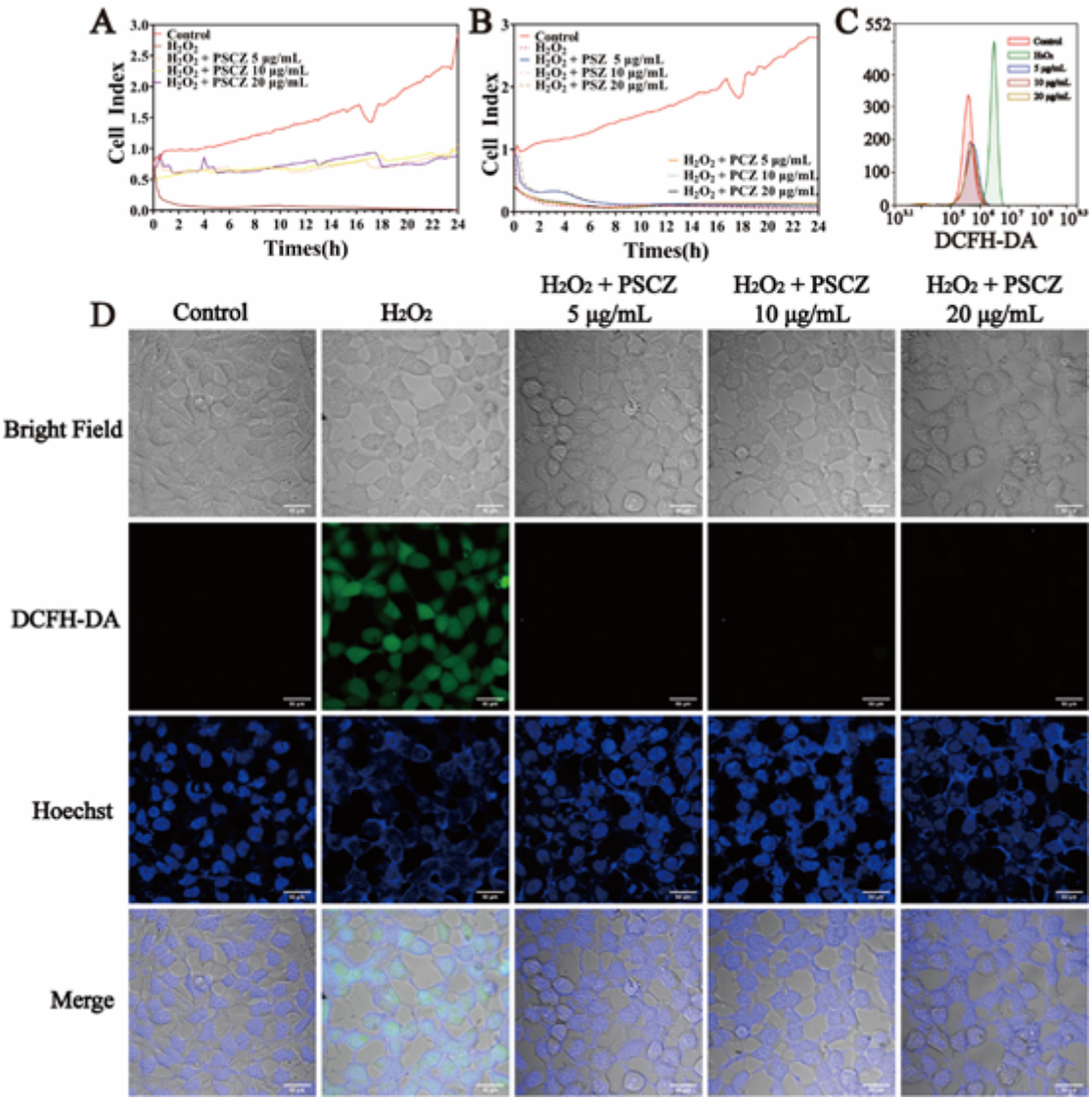

Figure 2

Assessment of the in vitro ROS scavenging activity of PSCZ. A-B) An xCELLigence (RTCA) platform was used to assess HEK293 cell treatment following treatment with H2O2 (200μm) and the indicated free enzymes (A) or PSCZ (B). C) ROS levels were assessed in HEK293 cells treated with the indicated concentrations of PSCZ and H2O2 (200 μm). D) Representative images of HEK293 cell ROS staining (green) in the indicated treatment groups, with nuclei being stained using DAPI (blue).

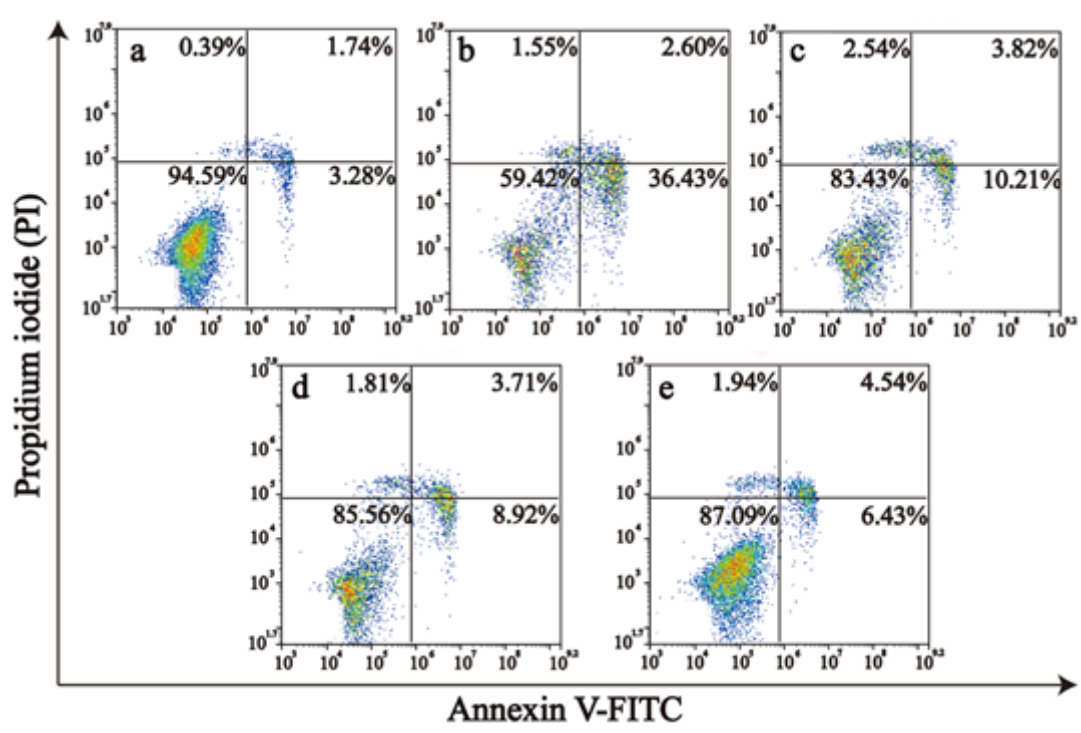

Figure 3

PSCZ protects HEK293 cells against oxidative damage induced by H2O2. AnnexinV–fluorescein isothiocyanate (FITC)/PI dual-staining was used to assess the impact of various PSCZ concentrations on apoptotic cell death in HEK293 cells that had been treated for 24 h with H2O2 (200 μm). a) Control group; b) H2O2 treatment (200 μm); c) H2O2 (200 μm)+PSCZ 5 μg/mL; d) H2O2 (200 μm)+PSCZ 10 μg/mL; e) H2O2 (200 μm)+PSCZ 20 μg/mL.

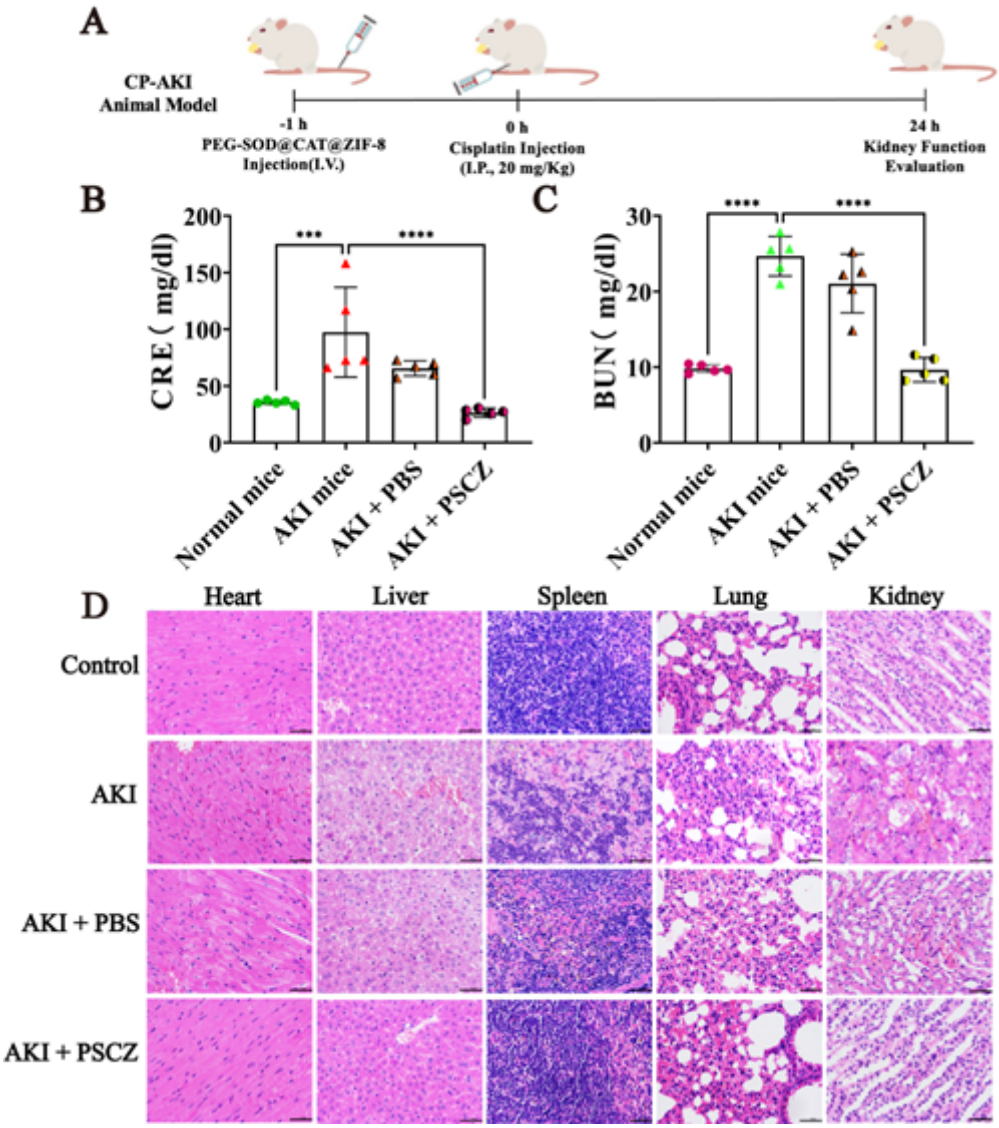

Figure 4

Assessment of the biocompatibility of PSCZ in vivo. A) CP-AKI modeling approach. B) CRE levels in CP-AKI mice were measured at 24 h following the indicated treatments. C) BUN levels in CP-AKI mice were measured at 24 h following the indicated treatments. D) Tissues from the indicated treatment groups were assessed following H&E staining.

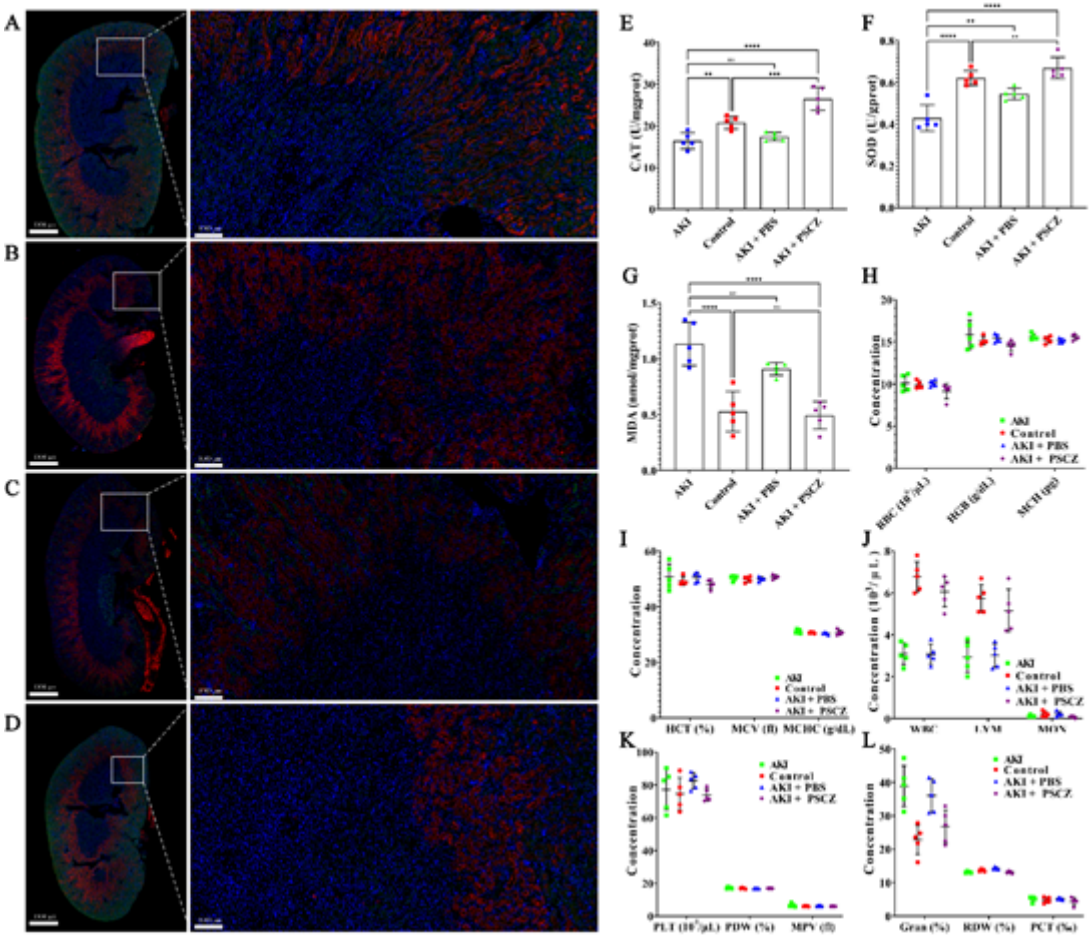

Figure 5

Analysis of renal biomarker expression and ROS accumulation. A-D) TNF-α and IL-1β levels in mice from the indicated treatment groups were detected via immunofluorescent staining. (A) Control; (B) CP-AKI; (C) CP-AKI+PBS; (D) CP-AKI+PSCZ; E) CAT levels in renal homogenates; F) SOD levels in kidney homogenates; G) MDA levels for mice in the indicated groups; H-L) The indicated hematological parameters were assessed in murine treatment groups at 24 h post-PSCZ injection.

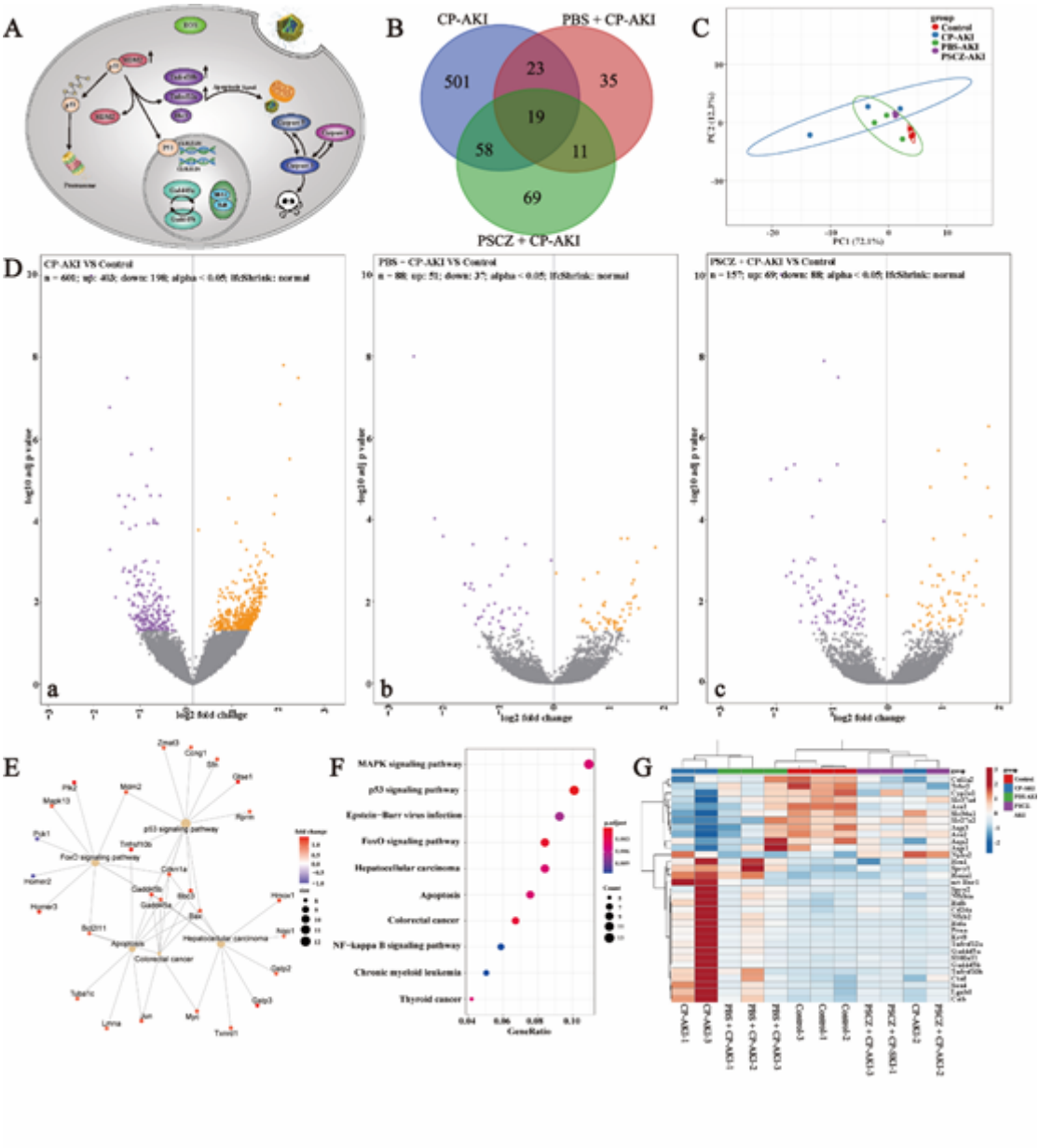

Figure 6

Analysis of transcriptome sequencing results. A) Mechanism of the figure; B) Venn diagram of the transcriptomic profiles between CP-AKI, PBS +CP-AKI, PSCZ+CP-AKI groups; C) Principal component analysis (PCA) was performed based on differentially expressed genes from the kidneys of two groups. Each data point corresponds to the PCA analysis of each sample; D) Volcano plots showing the identified upregulated and downregulated genes in each group; E) Gene mapping of differentially expressed genes involved in oxidative stress; F) KEGG pathway enrichment analysis of the identified differentially expressed genes; G) Upregulated and downregulated genes involved in the oxidative stress after PSCZ treatment.

Supplementary Files

This is a list of supplementary files associated with this preprint. Click to download.

- Supportinformation.docx